Oscillation Spectrum of a Magnetized Strongly Coupled One-Component Plasma

T. Ott,[1] H. Kählert,[1] A. Reynolds,[1,2] and M. Bonitz[1]

[1]*Christian-Albrechts-Universität zu Kiel, Institut für Theoretische Physik und Astrophysik, Leibnizstraße 15, 24098 Kiel, Germany*
[2]*School of Physics and Astronomy, University of Birmingham, Edgbaston, Birmingham B15 2TT, United Kingdom*

(Received 23 December 2011; published 18 June 2012)

A first-principles study of the collective oscillation spectrum of a strongly correlated one-component plasma in a strong magnetic field is presented. The spectrum consists of six fundamental modes that are found to be in good agreement with results from the quasilocalized charge approximation. At high frequencies, additional modes are observed that include Bernstein-type oscillations and their transverse counterparts, which are of importance for the high-frequency optical and transport properties of these plasmas.

DOI: 10.1103/PhysRevLett.108.255002 PACS numbers: 52.27.Gr, 52.27.Lw, 52.35.Fp

Strongly coupled charged-particle systems in which the interaction energy exceeds the kinetic energy are of rapidly growing interest in many fields reaching from condensed matter to ultracold gases, trapped ions, nonideal plasmas up to the quark-gluon plasma (e.g., Ref. [1]). Quite often these systems are subject to a strong magnetic field—examples are white dwarf stars, neutron star crusts [2,3], magnetized target fusion scenarios [4,5], and quantum Hall systems [6]. Magnetic field effects are also coming into the focus of laboratory experiments with dusty plasmas [1], ultracold neutral plasmas [7], and trapped ions [8]. Apart from basic transport properties such as diffusion [9], the collective excitation spectra are of fundamental relevance, e.g., for the response to optical excitation. In two-dimensional (2D) plasmas, the properties of these wave spectra are firmly established analytically via the quasilocalized charge approximation (QLCA) of Kalman and Golden [10–12] and computer simulations [13]. Strong correlations lead to the existence of a shear-type mode [14,15] alongside the familiar compressional modes (plasmons) known from weakly coupled situations. These shear modes could be verified in 2D dusty plasma experiments [16,17]. In the presence of a strong magnetic field, these transform into two modes commonly known as magnetoplasmon and magnetoshear, or upper and lower hybrid mode (e.g., see Ref. [18]).

Surprisingly, the corresponding behavior of the much more common strongly coupled three-dimensional plasmas has remained unexplored, except for a preliminary study in Ref. [19]. The present work is, therefore, devoted to filling this gap by a theoretical approach based on the QLCA and complementary first-principle molecular dynamics (MD) simulations. We obtain the complete set of fundamental linear oscillations and explore their wave-vector dispersion and polarization. Furthermore, we present evidence for the existence of nonlinear modes that are generalizations of Bernstein modes of high-temperature plasmas [20,21].

Model and simulation method.—We consider a classical one-component plasma (with a neutralizing homogeneous background, OCP) subject to an external magnetic field $\mathbf{B} = B\hat{\mathbf{e}}_z$. The exact equations of motion for N particles are

$$\ddot{\mathbf{r}}_i = \mathbf{F}_i/m + \omega_c \mathbf{v}_i \times \hat{\mathbf{e}}_z, \qquad i = 1 \ldots N, \tag{1}$$

where $\mathbf{v}_i = \dot{\mathbf{r}}_i$ and F_i is the Coulomb force due to all particles $j \neq i$. The thermodynamic equilibrium state of the system is characterized by the coupling parameter $\Gamma = q^2 \times (4\pi\varepsilon_0 a k_B T)^{-1}$, where $a = [3/(4n\pi)]^{1/3}$ is the Wigner-Seitz radius with the number density n and q denotes the particle charge. The strength of the magnetic field B is given by $\beta = \omega_c/\omega_p \propto B$, i.e., the ratio of the cyclotron frequency $\omega_c = qB/m$ and the plasma frequency $\omega_p^2 = nq^2/(\varepsilon_0 m)$. The spectra of the longitudinal and transverse fluctuations, $L(k, \omega)$ and $T(k, \omega)$, of the OCP follow from the Fourier component of the general current density operator in standard manner [22,23]:

$$\mathbf{j}(k, t) = \sum_{j=1}^{N} \mathbf{v}_j(t) \exp[i\mathbf{k} \cdot \mathbf{r}_j(t)], \tag{2}$$

via a temporal Fourier transform $\mathcal{F}_t$

$$\frac{1}{2\pi N} \lim_{t\to\infty} \frac{1}{t} |\mathcal{F}_t\{\mathbf{j}(k, t)\}|^2. \tag{3}$$

The current can be decomposed into a part parallel and a part perpendicular to $\mathbf{k}$, $\mathbf{j} = \mathbf{j}_\parallel + \mathbf{j}_\perp$, so application of Eq. (3) to $\mathbf{j}_\parallel$ yields the longitudinal spectrum $L(k, \omega)$ and to $\mathbf{j}_\perp$ the transverse spectrum $T(k, \omega)$. Collective oscillations appear as peaks in these spectra (Fig. 1).

Zero magnetic field.—To set the stage, consider first the unmagnetized system. In Fig. 1, we plot the longitudinal and transverse fluctuation spectra $L(k, \omega)$ and $T(k, \omega)$ together with the well-known QLCA results for the collective modes (solid black lines [14,24]). There are two remarkable deviations from the familiar spectrum of a weakly coupled plasma (e.g., Refs. [20,25]). First, the plasmon dispersion does not show a monotonic increase as $\omega^2(k) = \omega_p^2(1 + 3k^2 r_D^2)$ [r_D is the Debye radius] but decays and exhibits oscillations. Second, there exists an additional shear mode in the transverse spectrum. Figure 1

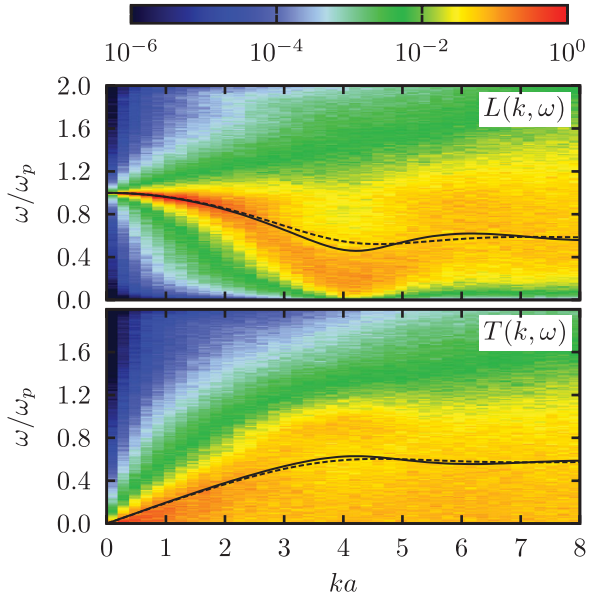

FIG. 1 (color). Longitudinal spectrum $L(k, \omega)$ and transverse spectrum $T(k, \omega)$ of an unmagnetized OCP at $\Gamma = 100$. The black lines are the QLCA dispersion relations (plasmon and ordinary shear mode) for $\Gamma = 100$ (solid line) and $\Gamma = 20$ (dashed line).

also shows that the precise value of Γ is of minor importance; increase of the coupling tends to slightly increase the amplitude of the oscillations. Overall, Fig. 1 indicates that QLCA describes the oscillation spectrum of a strongly coupled OCP rather well [26].

Theory for a magnetized OCP.—We now turn to a theoretical description of the wave spectrum in a magnetized strongly correlated OCP using the QLCA approach (e.g., Refs. [10,11,24]). The equation of motion for the collective coordinates $\eta_{\mathbf{k}\alpha}(\omega)$ in the presence of a magnetic field reads

$$\left[\omega^2\delta_{\alpha\beta} - D_{\alpha\beta}(\mathbf{k}) - \frac{k_\alpha k_\beta}{k^2}\omega_p^2 + i\omega\omega_c\sigma_{\alpha\beta}\right]\eta_{\mathbf{k}\alpha}(\omega) = 0, \quad \text{where } \sigma = \begin{pmatrix} 0 & -1 & 0 \\ 1 & 0 & 0 \\ 0 & 0 & 0 \end{pmatrix}, \tag{4}$$

and $D_{\alpha\beta}$ is the QLCA dynamical matrix [28], which is a functional of the pair distribution function $g(r)$. The nontrivial solutions to Eq. (4) represent the modes of the system, which turn out be rather complicated. Therefore, here we concentrate on modes with $\mathbf{k} \parallel \mathbf{B}$ or $\mathbf{k} \perp \mathbf{B}$. Their main properties are summarized in Tab. I and the dispersions are depicted for three different magnetic field strengths at strong coupling ($\Gamma = 100$) in Fig. 2. Obviously, there exist five possible (pairwise parallel or perpendicular) orientations of the vectors $\mathbf{B}$, $\mathbf{k}$, and $\mathbf{r}$—two (three) of them corresponding to $\mathbf{k} \parallel \mathbf{B}$ ($\mathbf{k} \perp \mathbf{B}$), cf. Table I. At the same time, the QLCA equation (4) yields six fundamental solutions—three for each orientation of the wave vector—which we discuss in the following.

Wave vector parallel to $\mathbf{B}$.—The three solutions of this type (black lines in Fig. 2) are the longitudinal plasmon (P), which is unaffected by the magnetic field since the particles oscillate parallel to $\mathbf{B}$, and two shear-mode solutions: upper and lower shear (US and LS). The latter arise from the shear mode of an unmagnetized plasma, cf. Fig. 1, whose degeneracy is lifted by the magnetic field. Their frequency difference equals ω_c (cf. Table I) and thus grows linearly with B.

Wave vector perpendicular to $\mathbf{B}$.—The three solutions (red lines in Fig. 2) are the ordinary shear mode (OS) and the upper and lower hybrid modes (UH and LH). The ordinary shear mode is B independent since the particle oscillation occurs along $\mathbf{B}$. The long-wavelength limit of the UH (LH) mode is $\omega = (\omega_p^2 + \omega_c^2)^{1/2}$ ($\omega = 0$). These two modes have peculiar polarization properties. While all four other modes are characterized by a fixed orientation of the displacement vector relative to $\mathbf{k}$—there are one longitudinal (P) and three transverse oscillations (US, LS, OS)— the UH and LH modes exhibit particle oscillations that rotate with time elliptically in the plane perpendicular to $\mathbf{B}$. To clarify these properties, the bottom part of Fig. 2 shows the modified eccentricity $\varepsilon = \gamma\sqrt{1 - b^2/a^2}$, where the semimajor axis $a = \max\{|\eta_x|, |\eta_y|\}$, the semiminor axis $b = \min(|\eta_x|, |\eta_y|)$, and γ equals 1 if $\eta_x > \eta_y$ and -1 otherwise. Here, $\vec{\eta}$ is the eigenvector of Eq. (4) for the solutions UH and LH, respectively. $\varepsilon = +1$ (-1) for

TABLE I. The six principal collective modes in a magnetized three-dimensional OCP in QLCA. Shown are the relative orientations of the wave vector $\vec{k}$, magnetic field $\vec{B}$, particle displacement $\vec{r}$, the wave type, the polarization, the dispersion relation $\omega_i(k)$, and its asymptotic ω_i^∞, for large k and the current spectrum in which they appear. $\omega_E = \omega_p/\sqrt{3}$ is the Einstein frequency, $D_{L/T}$ denotes the longitudinal and transverse parts of $D_{\alpha\beta}$, $\Omega_T^4 = [\Omega_L^2 - D_T(k)]^2 + 4\omega_c^2 D_T(k)$, and $\Omega_L^2 = \omega_p^2 + \omega_c^2 + D_L(k)$.

Name	$\vec{k}\angle\vec{B}$	$\vec{r}\angle\vec{B}$	$\vec{k}\angle\vec{r}$	Type	Polarization	Dispersion $\omega_i(k)$	Asymptotic ω_i^∞	Spectrum
Plasmon (P)	$\parallel$	$\parallel$	$\parallel$	longit.	not applicable	$\sqrt{\omega_p^2 + D_L(k)}$	ω_E	$L^\parallel$
Upper Shear (US)	$\parallel$	$\perp$	$\perp$	transv.	circular	$\frac{1}{2}[\sqrt{\omega_c^2 + 4D_T(k)} + \omega_c]$	$\frac{1}{2}[\sqrt{\omega_c^2 + 4\omega_E^2} + \omega_c]$	$T_\parallel^\perp$
Lower Shear (LS)	$\parallel$	$\perp$	$\perp$	transv.	circular	$\frac{1}{2}[\sqrt{\omega_c^2 + 4D_T(k)} - \omega_c]$	$\frac{1}{2}[\sqrt{\omega_c^2 + 4\omega_E^2} - \omega_c]$	$T_\parallel^\perp$
Ordinary Shear (OS)	$\perp$	$\parallel$	$\perp$	transv.	linear	$\sqrt{D_T(k)}$	ω_E	$T^\parallel$
Upper Hybrid (UH)	$\perp$	$\perp$	t-dep.	hybrid	in-plane elliptical	$\frac{1}{\sqrt{2}}[\Omega_L^2 + D_T(k) + \Omega_T^2]^{1/2}$	$\frac{1}{2}[\sqrt{\omega_c^2 + 4\omega_E^2} + \omega_c]$	$L^\perp + T_\perp^\perp$
Lower Hybrid (LH)	$\perp$	$\perp$	t-dep.	hybrid	in-plane elliptical	$\frac{1}{\sqrt{2}}[\Omega_L^2 + D_T(k) - \Omega_T^2]^{1/2}$	$\frac{1}{2}[\sqrt{\omega_c^2 + 4\omega_E^2} - \omega_c]$	$L^\perp + T_\perp^\perp$

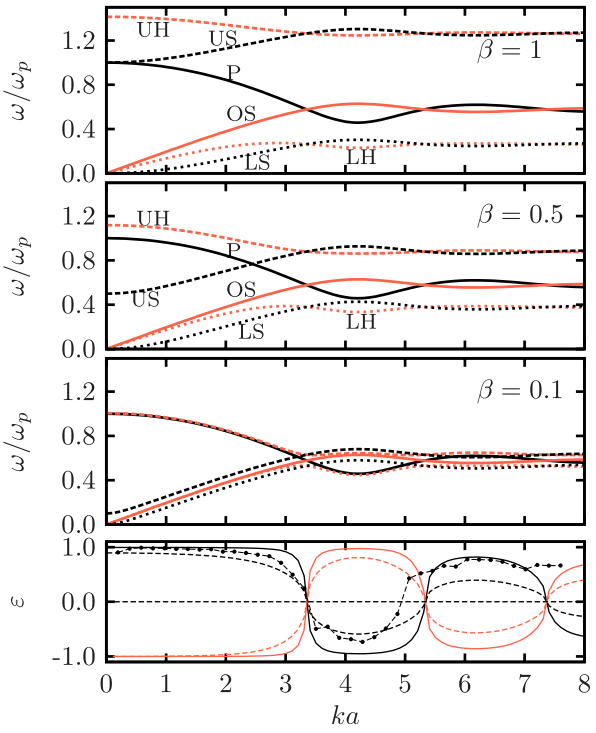

FIG. 2 (color online). The modes of a 3D magnetized OCP ($\kappa = 0$, $\Gamma = 100$) in QLCA: plasmon (P), ordinary shear (OS), upper hybrid (UH), lower hybrid (LH), lower shear (LS), and upper shear (US), for three magnetic field strengths. Modes with $\mathbf{k} \parallel \mathbf{B}$ are shown in black (dark), and those with $\mathbf{k} \perp \mathbf{B}$ in red (light). Bottom: k dependence of the eccentricity ε of the UH (black) and LH (red) for $\beta = 0.1$ (solid) and $\beta = 0.5$ (dashed). Simulation results are shown by the symbols for the UH mode at $\Gamma = 100$ and $\beta = 0.5$.

longitudinal (transverse) waves. Moreover, the shape of this ellipse is k dependent, cf. Fig. 2 [29]. The UH mode starts longitudinal at long wavelengths and transforms into a predominantly transverse wave at the first crossing of the P and OS modes. At each subsequent crossing point, the dominant character of the wave changes again. The LH mode exactly mirrors this behavior. For $k \to \infty$, both modes are in-plane circular. The limit $B \to 0$ of these modes is particularly interesting: while all six modes converge to the two modes shown in Fig. 1, the LH and UH modes only do so in a pointwise manner. The LH, at all k, remains below the UH; i.e., we observe an avoided crossing of the two at the intersection points of the plasmon and shear mode (see the case $\beta = 0.1$ in Fig. 2).

Simulation results.—Let us now critically test the theoretical predictions against the computer experiment. To this end, Eq. (1) is solved by a microcanonical MD method for $N = 8000$ particles, incorporating an arbitrarily strong static homogeneous magnetic field into the second-order Velocity Verlet algorithm [30]. Prior to data acquisition, the system is equilibrated by an isokinetic thermostat. The above mentioned five possible orientations of **B**, **k**, and **r** manifest themselves in five different currents of the type (2), leading to five fluctuation spectra: there are two longitudinal ones, $L^{\parallel}$ and $L^{\perp}$ (the superscript denotes the mutual orientation of **B** and **r**) and three transverse ones, $T^{\parallel}$, $T^{\parallel}_{\parallel}$ and $T^{\parallel}_{\perp}$ (the subscript specifies the angle between **B** and **k** in case of an ambiguity). The correspondence of the five fluctuation spectra to the six collective oscillations can be seen in Table I.

Figure 3 shows the wave spectra of a magnetized OCP at $\Gamma = 100$ and $\beta = 1.0$. To capture the two hybrid modes, the two spectra $L^{\perp}(k, \omega)$ and $T^{\perp}_{\perp}(k, \omega)$ have been added together. Six frequency peaks can be identified whose position and full width at half maximum (FWHM) are indicated in the figure at selected values of ka. Overall, a

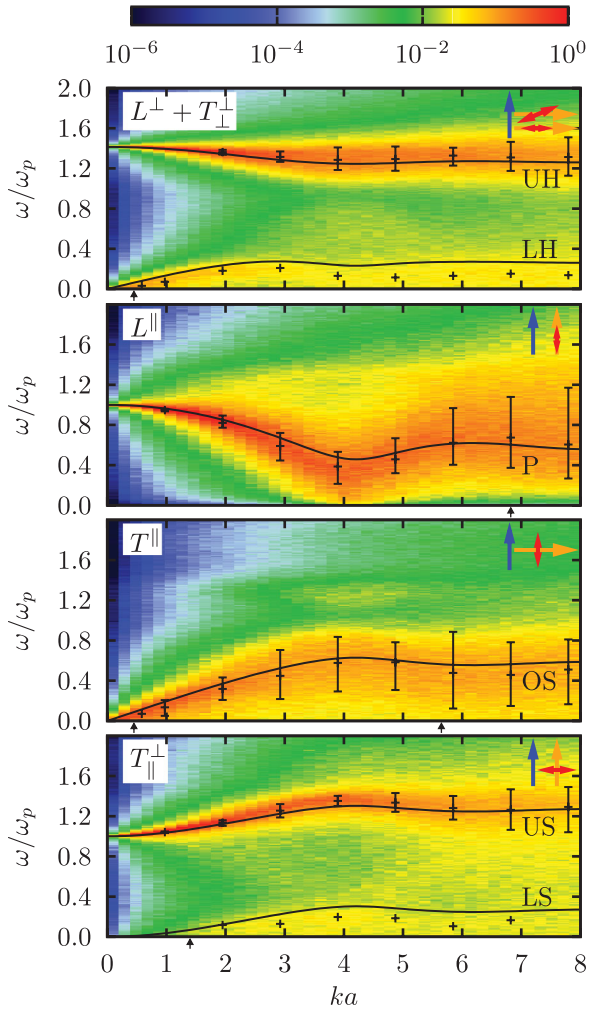

FIG. 3 (color). The complete set of oscillation spectra of a magnetized OCP at $\Gamma = 100$ and $\beta = 1.0$ for frequencies $\omega \leq 2\omega_p$. The solid lines correspond to the six QLCA modes that are labeled in the figure, cf. Tab. I. The orientation of the magnetic field (blue), wave vector (orange), and particle oscillations (red) are indicated by the large arrows. The small arrows on the abscissa indicate the positions at which the peaks vanish at small k and at which k the wave frequency equals the FWHM of the peak (given by the "error" bars), respectively.

good agreement with the QLCA modes is evident. Similarly, the eccentricity ϵ of the UH mode observed in the simulation agrees well with the QLCA predictions for $ka \lesssim 5$ (lower panel of Fig. 2). These conclusions are representative and hold also for other values of Γ and β. At the same time, there exist four noticeable deviations of the QLCA from the simulations. The first is observed at low frequencies (corresponding to long times) due to the breakdown of the QLCA assumption of a frozen potential landscape [12]. Second, the low-frequency shear modes vanish at small k (see small arrows in Fig. 3), which is not reproduced in QLCA [31,32]. Third, the QLCA does not include damping and thus no information about the domain of existence of the waves in the k space can be accessed, in contrast to the simulations (small arrows in Fig. 3). Finally, it has been observed that QLCA misses the high-frequency part of the spectrum in a 2D magnetized OCP, where Bernstein-type modes were found in the simulations [33,34]. It is, therefore, tempting to analyze in more detail the frequency region that is not captured by Fig. 3.

In the left column of Fig. 4, we present the high-frequency part of the $\mathbf{B} \perp \mathbf{k}$ spectra. In addition to the UH and LH modes, for $\beta \gtrsim 0.5$ the spectrum $L^{\perp} + T_{\perp}^{\perp}$ exhibits a number of equally spaced further peaks that clearly resemble Bernstein modes of high-temperature plasmas (e.g., Ref. [20,21]). In a 2D OCP it was found recently that "dressed" (modified by correlations) Bernstein modes reappear at strong coupling [33,34]. The analysis of the present 3D spectra shows that these modes appear at multiples of the high-k limit of the upper shear and upper hybrid frequency (see the asymptotics in Table I), $\omega_{\mathrm{UH}}^{\infty} = \omega_{\mathrm{US}}^{\infty} \equiv \omega_{\infty} = \frac{1}{2}[(\omega_c^2 + 4\omega_E^2)^{1/2} + \omega_c]$, with the Einstein frequency $\omega_E = \omega_p/\sqrt{3}$.

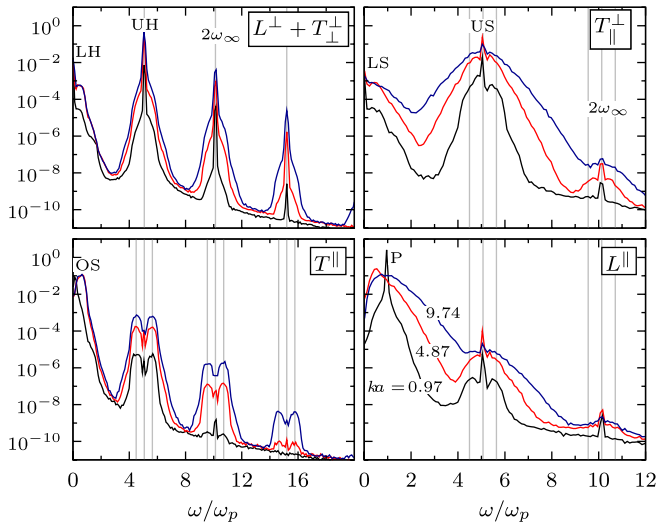

FIG. 4 (color online). Fluctuation spectra of an OCP extended to high frequencies, for $\beta = 5$ and three wave numbers, as indicated in the figure ($ka = 9.74, 4.87, 0.97$ from top to bottom line). Vertical lines indicate the harmonics $n\omega_\infty$ and the frequencies $n\omega_\infty \pm \omega_E$.

Apart from this similarity to a 2D OCP, the spectrum in 3D is much richer, and the harmonics $n\omega_\infty$ show up also in other fluctuations. Indeed, as can be seen in the lower left part of Fig. 4, the harmonics emerge also in the spectrum $T^{\parallel}$ around the same frequencies (solid gray lines). However, these peaks are visible only at small ka, whereas at higher ka a double-peak structure emerges at $n\omega^{\infty} \pm \omega_E$. This structure is accompanied by a broadening of the higher harmonics peaks in $L^{\perp}(\omega) + T_{\perp}^{\perp}(\omega)$ that develop "shoulders" around $n\omega_\infty \pm \omega_E$. A similar trend is observed in the two $\mathbf{B} \parallel \mathbf{k}$ excitation spectra, cf. right column of Fig 4. Here, the US mode is clearly seen in $T_{\parallel}^{\perp}(\omega)$ as a peak around $\omega/\omega_p \approx 5$. Additionally, the second harmonic of the US is visible around $\omega/\omega_p \approx 10$. These two peaks also appear in $L^{\parallel}(\omega)$, alongside the low-frequency plasmon peak at $\omega/\omega_p \approx 1/\sqrt{3}$, cf. Table I. The peaks at $\omega/\omega_p \approx 5$, 10 are accompanied by the same double-peak structure seen in the cross-field wave spectra.

All of these high-frequency features can be understood within a common simple physical picture: scattering of multiple short wavelength oscillations where $\omega_1 + \omega_2 = \omega_{12}$ and $\mathbf{k}_1 + \mathbf{k}_2 = \mathbf{k}_{12}$, a well-known mechanism in high-temperature plasmas [20,25] and nonlinear optics. In fact, the nth harmonic of the US (UH) is explained by a cascade of nonlinear inelastic interactions $\omega_\infty \rightarrow 2\omega_\infty \rightarrow \ldots n\omega_\infty$. On the other hand, the pair of side peaks at $\omega_\infty \pm \omega_E$ in the left column of Fig. 4 arise from the scattering of an UH (frequency ω_∞) with an OS wave (frequency ω_E), and the analogous peaks in the right column of Fig. 4 are due to a scattering of an US mode and a plasmon (frequencies ω_∞ and ω_E). Finally, the appearance of the peaks at $\omega/\omega_p \approx 5$, 10, 15 in $T^{\parallel}$ (at $\omega/\omega_p \approx 5$, 10 in $L^{\parallel}$) are due to elastic scattering of an UH (US) mode (or a corresponding higher harmonic) with that frequency during which the particle oscillation direction is turned from in-plane ($\perp \mathbf{B}$) to out-of-plane ($\parallel \mathbf{B}$), which requires a finite shear elasticity—a remarkable feature of strongly correlated plasmas [35]. It is particularly striking that this mechanism also excites novel longitudinal modes in the plasmon spectrum $L^{\parallel}$ that have a B-dependent frequency, in contrast to the fundamental plasmon.

In summary, we have presented the complete collective oscillation spectrum of a strongly correlated one-component plasma in a magnetic field. The OCP supports six base modes—three for each $\mathbf{k}$—that are well described by the QLCA, as well as additional oscillations arising from elastic and inelastic wave scattering. They are fueled by the familiar Bernstein scenario of harmonics generation in a magnetic field, but their base frequency is modified by correlations and differs from ω_c. Furthermore, correlations give rise to a novel class of modes: transverse Bernstein

waves, which are harmonics of the upper shear oscillation. The present results are representative for a broad range of coupling parameters and for Coulomb and Yukawa OCP as well. They are, therefore, expected to be of direct relevance for the high-frequency transport and optical response of a broad spectrum of strongly coupled magnetized plasmas—from white dwarf and neutron stars to trapped ions and dusty plasmas.

This work is supported by the DFG via SFB-TR 24 via projects A5 and A7, the DAAD via the RISE program, and a grant for CPU time at the North-German Supercomputing Alliance HLRN.

[1] M. Bonitz, C. Henning, and D. Block, Rep. Prog. Phys. **73**, 066501 (2010).
[2] F. Peng, E. F. Brown, and J. W. Truran, Astrophys. J. **654**, 1022 (2007).
[3] D. A. Baiko, Phys. Rev. E **80**, 046405 (2009).
[4] M. Basko, A. Kemp, and J. M. ter Vehn, Nucl. Fusion **40**, 59 (2000).
[5] C. Deutsch and R. Popoff, Nucl. Instrum. Methods Phys. Res., Sect. A **606**, 212 (2009).
[6] S. V. Tovstonog *et al.*, Phys. Rev. B **66**, 241308(R) (2002).
[7] T. Killian, T. Pattard, T. Pohl, and J. Rost, Phys. Rep. **449**, 77 (2007).
[8] A. Dantan, J. P. Marler, M. Albert, D. Guénot, and M. Drewsen, Phys. Rev. Lett. **105**, 103001 (2010).
[9] T. Ott and M. Bonitz, Phys. Rev. Lett. **107**, 135003 (2011).
[10] K. I. Golden, G. Kalman, and P. Wyns, Phys. Rev. B **48**, 8882 (1993).
[11] K. Jiang, Y.-H. Song, and Y.-N. Wang, Phys. Plasmas **14**, 103708 (2007).
[12] G. Kalman, K. Golden, Z. Donko, and P. Hartmann, J. Phys.: Conf. Proc. **11**, 254 (2005).
[13] L.-J. Hou, P. K. Shukla, A. Piel, and Z. L. Mišković, Phys. Plasmas **16**, 073704 (2009).
[14] Z. Donkó, G. J. Kalman, and P. Hartmann, J. Phys. Condens. Matter **20**, 413101 (2008).
[15] N. Upadhyaya, V. Nosenko, Z. L. Mikovi, L.-J. Hou, A. V. Ivlev, and G. E. Morfill, Europhys. Lett. **94**, 65001 (2011).
[16] J. B. Pieper and J. Goree, Phys. Rev. Lett. **77**, 3137 (1996).
[17] A. Piel, V. Nosenko, and J. Goree, Phys. Plasmas **13**, 042104 (2006).
[18] G. Uchida, U. Konopka, and G. Morfill, Phys. Rev. Lett. **93**, 155002 (2004).
[19] G. Kalman, K. I. Golden, and M. Minella, in *Strongly Coupled Plasma Physics*, edited by H. M. Van Horn and S. Ichimaru (University of Rochester Press, Rochester, 1994).
[20] P. Bellan, *Fundamentals of Plasma Physics* (Cambridge University Press, Cambridge, England, 2006).
[21] I. B. Bernstein, Phys. Rev. **109**, 10 (1958).
[22] J. P. Hansen, I. R. McDonald, and E. L. Pollock, Phys. Rev. A **11**, 1025 (1975).
[23] J. Boon and S. Yip, *Molecular Hydrodynamics* (Courier Dover Publications, New York, 1991).
[24] G. Kalman and K. I. Golden, Phys. Rev. A **41**, 5516 (1990).
[25] A. F. Alexandrov, L. S. Bogankevich, and A. A. Rukhadse, *Principles of Plasma Electrodynamics* (Springer, Berlin, 1984).
[26] The occurrence of a two-peak structure around $ka = 4$ in the simulations is attributed to the emerging short-ranged "microcrystalline" order and differences in wave propagation along the "crystal" axes. QLCA gives an average frequency and is unable to resolve such features. A similar observation has been made in Ref. [27] for two-dimensional systems.
[27] L.-J. Hou, Z. L. Mišković, A. Piel, and M. S. Murillo, Phys. Rev. E **79**, 046412 (2009).
[28] K. I. Golden and G. J. Kalman, Phys. Plasmas **7**, 14 (2000).
[29] A similar behavior has been observed for a 2D plasma crystal in a magnetic field in Ref. [18].
[30] Q. Spreiter and M. Walter, J. Comput. Phys. **152**, 102 (1999).
[31] H. Ohta and S. Hamaguchi, Phys. Rev. Lett. **84**, 6026 (2000).
[32] M. S. Murillo, Phys. Rev. Lett. **85**, 2514 (2000).
[33] M. Bonitz, Z. Donkó, T. Ott, H. Kählert, and P. Hartmann, Phys. Rev. Lett. **105**, 055002 (2010).
[34] T. Ott, M. Bonitz, P. Hartmann, and Z. Donkó, Phys. Rev. E **83**, 046403 (2011).
[35] Another manifestation of the shear elasticity is the coupling of diffusion perpendicular and parallel to the magnetic field [9].